the online version of record will be different from this version once it has been copyedited and typeset

PLEASE CITE THIS ARTICLE AS DOI: 10.1063/5.0216515

This is the author's peer reviewed, accepted manuscript. However,

### Signatures of Coherent Vibrational Dynamics in Ethylene Carbonate

Luke Guerrieri, Sarah Hall, Brad M. Luther, and Amber T. Krummel\*

Electronic Mail: Amber.Krummel@colostate.edu

### **AFFILIATIONS**

Department of Chemistry, Colorado State University, Fort Collins, Colorado 80523, USA

Abstract: Despite having practical applications in battery technology and serving as a model system for Fermi resonance coupling, ethylene carbonate (EC) receives little direct attention as a vibrational probe in nonlinear vibrational spectroscopy experiments. EC contains a Fermi resonance which is well characterized in the linear spectrum, and the environmental sensitivity of its Fermi resonance peaks could make it a good molecular probe for two-dimensional infrared spectroscopy (2DIR) experiments. As a model system, we investigate the linear and 2DIR vibrational spectrum of the carbonyl stretching region of ethylene carbonate in tetrahydrofuran (THF). The 2DIR spectrum reveals peak dynamics which evolve coherently. We characterize these dynamics in the context of Redfield theory and find evidence that EC dynamics proceed through coherent pathways, including singular coherence transfer pathways which have not been widely observed in other studies. We find that coherent contributions play a significant role in the observed dynamics of cross peaks in the 2DIR spectrum which must be accounted for to extract accurate measurements of early waiting time dynamics.

### I. Introduction

As the need for safer and more efficient energy storage devices grows, an increasing amount of research has been dedicated to understanding the underlying molecular physics dictating the function of battery technologies. <sup>1–6</sup> Linear and time dependent nonlinear vibrational spectroscopies have been increasingly employed as a means of studying the structure and dynamics of electrolyte solutions relevant to battery performance, with a fair amount of attention given to organic electrolytes composed of mixtures of linear and cyclic carbonates commonly found in commercial lithium-ion batteries. <sup>1,2,4–13</sup> Ion solvation primarily occurs through interaction with the carbonyl mode of the electrolyte components, <sup>1,2,10,12</sup> so it is desirable to probe the carbonyl stretching region directly. As such the carbonyl stretching regions of several organic carbonates have been used as molecular probes in 2DIR experiments to gain insight on the role of the electrolyte in device function. Ethylene carbonate (EC) is a common component of these

PLEASE CITE THIS ARTICLE AS DOI: 10.1063/5.0216515

### mixtures, but time dependent vibrational studies which directly study EC are overall scarce, <sup>13</sup> and to our knowledge, nonexistent for the carbonyl region. One stated reason for this is due to the presence of an additional Fermi resonance band<sup>2</sup> in the carbonyl region which contributes to spectral congestion. That same Fermi resonance makes EC a model compound for linear IR and Raman studies of Fermi resonance coupling. <sup>14–18</sup> Time dependent IR studies show that coherent excitations of Fermi doublets introduce oscillations in peak intensities which may obscure underlying population dynamics. <sup>19–22</sup> However, coherent oscillations in peak intensities are also a signature of coherent vibrational energy transfer (CVET). <sup>23–26</sup> This raises the possibility that

studies of Fermi resonance coupling. 14–18 Time dependent IR studies show that coherent excitations of Fermi doublets introduce oscillations in peak intensities which may obscure underlying population dynamics. 19–22 However, coherent oscillations in peak intensities are also a signature of coherent vibrational energy transfer (CVET). 23–26 This raises the possibility that the coherent oscillations observed in 2DIR spectra of Fermi resonances could result from CVET pathways, in which case they reflect important elements of the system dynamics. To our knowledge there have been no time dependent vibrational studies directly investigating the extent of CVET in Fermi coupled systems. Theoretical models of coherent energy transfer often assume the coupling of coherence states is facilitated by coupling to bath coordinates. This could be of particular importance in studies of organic battery electrolytes which use carbonyl transitions of a particular solvent element as an IR probe. Moreover, the bath in the organic electrolyte cocktail is a sea of carbonates. In this case the presence of energetically similar transitions in the electrolyte and the IR probe may provide a mechanism for coherent dynamics.

To assess the viability of EC as an IR probe molecule we set out to characterize the 2DIR spectrum of EC using tetrahydrofuran (THF) as a model solvent. THF has previously been used as a model solvent in studies of linear carbonates coordinated to lithium ions, as it has some similar dielectric properties to linear carbonates used in battery electrolytes.<sup>4</sup> In this system we detect clear signatures of coherent excitations and interpret them in the context of nonsecular Redfield theory.<sup>27,28</sup> Nonsecular Redfield theory allows for additional relaxation pathways in which coherent superpositions of system eigenstates couple to other coherences or to population states.<sup>27,29–31</sup> This framework has been employed<sup>31,32</sup> to describe long lived coherences observed in time dependent electronic spectra of photosynthetic pigments<sup>33,34</sup> and was recently utilized to identify vibrational energy transport to IR-inactive modes in a 2DIR study of metal carbonyl compounds. <sup>24</sup> The spectral signatures of nonsecular relaxation are well characterized by joint theoretical and experimental 2DIR studies,<sup>23,26</sup> and those signatures are easily understood by incorporating nonsecular relaxation into the well-known Feynman diagram representation of third order response functions. In this framework coherent oscillations in peak intensities are directly related to features in the linear and 2DIR spectra. Within the context of

PLEASE CITE THIS ARTICLE AS DOI: 10.1063/5.0216515

### Redfield theory, we compare the frequency positions of oscillating peaks in rephasing and non-rephasing spectra to confirm the presence of CVET. We then use pump selective experiments to characterize the CVET contributions to features in the 2DIR spectrum.

### **II. Experimental Methods**

### Sample Preparation and Linear IR

Ethylene carbonate (EC) and tetrahydrofuran (THF) were purchased from Sigma-Aldrich and Oakwood Chemical, respectively. Both were used without further purification. We stored EC in a vacuum desiccator to avoid contamination from water. Samples for linear and 2DIR experiments consisted of 50-75 mM EC dissolved in THF. The solutions were sandwiched between a pair of 1 mm calcium fluoride (CaF2) plates (Crystran) with a diameter of 25.4 mm and a 25  $\mu$ m path length determined by a Teflon spacer (Harrick). We collected linear IR measurements with a Bruker Optics Vertex 70 spectrometer set to 64 scans and a resolution of 2 cm<sup>-1</sup>. Time dependent linear IR measurements indicated that the sample remained stable over a four-hour period, which served as the upper limit for collection of 2DIR data.

### 100 kHz 2DIR spectrometer

A home built OPCPA ultrafast laser system produced the 100 kHz mid-IR pulse train used in 2DIR experiments. The operating principles of the system have been described previously. These experiments utilized mid-IR pulses centered at 1750 cm<sup>-1</sup> with a FWHM of 214 cm<sup>-1</sup>. A  $\frac{\lambda}{2}$  waveplate and mid-IR thin film polarizer split the OPCPA output into pump and probe lines with tunable energy. Pulse energies at the sample were evenly divided between the two pump pulses and a single probe pulse, with an average of 0.1  $\mu$ J of energy per pulse.

### **2DIR Data Collection**

All 2DIR measurements took place in a partly collinear heterodyned pump-probe geometry<sup>38</sup> using a mid-IR pulse shaper (QuickShape+, PhaseTech Spectroscopy). Descriptions of 2DIR spectroscopy in this geometry are available elsewhere<sup>20,35,38,39</sup> and will not be described here. For clarity, we refer to  $t_1$  as the coherence time beginning at the interaction of the first pump pulse with the sample and terminating at the arrival of the second pump pulse. Similarly,  $t_2$  gives the waiting time of the experiment between pulses two and three, while  $t_3$  describes the final coherence period during which third order signal emits. Data collection utilized a 1x4 (2x2) phase cycling scheme<sup>40</sup> with a rotating frame of 1400 cm<sup>-1</sup> and  $t_1$  scan times ranging from 0 ps

This is the author's peer reviewed, accepted manuscript. However, the online version of record will be different from this version once it has been copyedited and typeset

PLEASE CITE THIS ARTICLE AS DOI: 10.1063/5.0216515

to 3 ps, 8 ps, or 10 ps. All  $t_1$  scans consisted of 401 steps; however, we found improved signal intensity when oversampling the earlier regions of our free induction decay. As such, we utilized varying  $t_1$  scan times to improve either  $t_1$  resolution or signal to noise in our limited experimental window. Because we find evidence the signatures of CVET are sensitive to  $t_1$ scan lengths, we do not directly compare the dynamics of data sets taken with different final  $t_1$ delays. SI.4 explores this result in more detail by using varying window functions to simulate different  $t_1$  scan times.

Fourier transform of the heterodyned 2DIR signal about  $t_3$  took place on a monochromator, and the frequency resolved signal was measured using a 64-element mercury cadmium telluride (MCT) array detector at 100 kHz (Infrared Systems.) The geometry of the 64element array and monochromator produced a spectral window spanning 1714-1849 cm<sup>-1</sup> with an approximate resolution of 2.1 cm<sup>-1</sup>. A mechanically controlled delay stage on the probe line yielded waiting time scans spanning either 0-6 ps or 0-15 ps. Scan times were chosen to optimize either signal to noise or the resolution of Fourier transforms over  $t_2$ . We employ a reference pixel noise reduction scheme<sup>41,42</sup> to limit the impact of probe noise on our spectra.

Data collection occurred in both the XXXX and XXYY polarization schemes<sup>39,43</sup> which were recombined to yield isotropic data sets presented in this work.<sup>20</sup> The free induction decay at each pixel was treated with an exponential window function for the final 2 ps of each scan, zero padded with an additional 401 steps, and normalized to the laser power. A Fourier transform along  $t_1$  generated the excitation axis  $\omega_1$ . All 2D spectra and kinetic traces presented in this work consist of the real Fourier transform of the signal. Rephasing and non-rephasing spectra were obtained according to methods outlined previously.<sup>44</sup> While it is more common to generate rephasing and non-rephasing signals from a 1x3 phase cycling scheme<sup>45</sup> we find that the purely absorptive spectrum obtained by combining the rephasing and non-rephasing signals agrees with the experimentally collected purely absorptive data.

### **Pump Selective 2DIR**

We employed pump selective 2DIR experiments to assess the significance of nonsecular relaxation in our system. We take advantage of the diffraction gratings in our pulse shaper to limit pump bandwidth, in line with previous experiments.<sup>25,40</sup> To maintain temporal resolution, we compress our pulses for both full and pump-selective experiments, which could cause variations in the pump pulse temporal profile. However, we do not detect significant differences in the dynamics of certain peaks (see SI.3) in the pump selective and full pump

PLEASE CITE THIS ARTICLE AS DOI: 10.1063/5.0216515

experiments. We take the consistency of these peak dynamics as indicating changes in the signal due to the pump temporal profile are not detectable within experimental error.

### III. Nonsecular Relaxation in 2DIR Spectroscopy

Signatures of coherent vibrational energy transfer in 2DIR spectra are well documented<sup>23,24,26,46</sup> and often addressed in the context of the Redfield equation<sup>27</sup> which we describe briefly.

$$\frac{\partial}{\partial t}\rho_{ab}(t) = -i\omega_{ab}\rho_{ab}(t) - \sum_{cd}\Gamma_{abcd}\rho_{cd}$$
(1)

Here  $\rho_{ab}$  is a given density matrix element,  $\omega_{ab}$  corresponds to the frequency of  $\rho_{ab}$ , and  $\Gamma_{abcd}$  is an element of the relaxation tensor which encodes information on the exchange of amplitude between  $\rho_{ab}$  and  $\rho_{cd}$ . Equation 1 results from a second order perturbative treatment which assumes weak system-bath coupling. $^{27,47-51}$  The secular approximation to Redfield theory assumes dynamical independence of the off-diagonal coherence ( $\rho_{ab}$ ) elements of the density matrix. In other words, coherence states do not exchange amplitude with other elements in the absence of an external force (such as a laser pulse). This leaves only the relaxation terms  $\Gamma_{aaaa}$ ,  $\Gamma_{aabb}$ , and  $\Gamma_{abab}$  which describe population relaxation, population transfer, and coherence dephasing, respectively. When incorporated into third order response theory, the secular approximation greatly reduces both the number of response pathways considered and the computational complexity of chemical dynamics simulations used to interpret 2DIR experiments.  $^{23,25,26,46}$ 

However, nonsecular relaxation may arise when bath interactions mutually couple a coherence state to other elements of the density matrix,  $^{24,46,52-56}$  resulting in coherent dynamics. To characterize CVET one may include the full Redfield tensor in 2DIR simulations.  $^{23,26,46,55,57,58}$  Such treatments explicitly consider Redfield tensor elements of the type  $\Gamma_{abac}$ ,  $\Gamma_{abcd}$ ,  $\Gamma_{abcc}$  and  $\Gamma_{aacd}$ . The first two terms describe coupling between coherences, and we refer to both as coherence transfer (CT). The last two terms describe coupling between populations and coherences. In both cases energy transfer occurs without a loss of phase information and is facilitated by mutual coupling to a bath coordinate. Timescales of these CVET processes follow the lifetime of the originating state. In the case of CT this corresponds to coherence dephasing times, while coherence-population coupling may occur over the coherence lifetime of the doubly excited state or the vibrational lifetime of the population. Joint theoretical and computational

PLEASE CITE THIS ARTICLE AS DOI: 10.1063/5.0216515

he Journal of

investigations identify several spectral signatures of CVET such as line broadening, 23,52 forbidden peaks at early waiting times,  $^{26,57}$  and additional oscillations in  $t_2$  peak dynamics. 23,24,46,57

Interpretations of these results are facilitated using Feynman diagrams which offer a convenient, if qualitative, means of accounting for CVET in 2DIR spectra. We present a handful of possible single-step CVET 2DIR pathways in Fig. 1(b,c). These pathways consider a system of four coupled oscillators with singly excited states denoted by  $|\alpha\rangle$ ,  $|\beta\rangle$ ,  $|\gamma\rangle$ , and  $|\epsilon\rangle$ . Secular diagrams for population transfer and quantum beating (QB) are given in Fig. 1(a) for comparison. The dashed horizontal lines in Fig. 1 indicate relaxation between states. To connect this representation to the above discussion, we include the Redfield tensor element for each dynamic response pathway. The upper two diagrams of Fig. 1(b) describe coherence transfer during the  $t_1$  coherence period, and analogous diagrams can be drawn for CVET occurring during  $t_3$ . CVET contributions to cross peaks at early waiting times can be visualized by  $t_1$  and

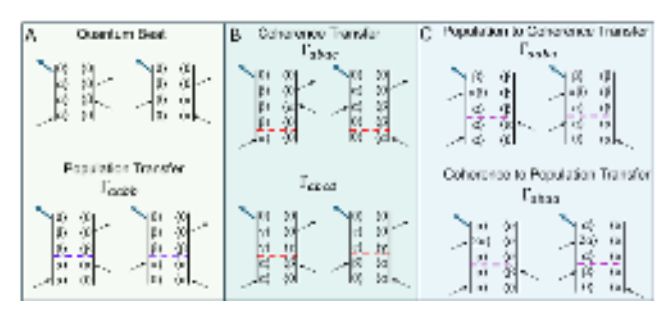


Fig 1. Examples of the Feynman diagram accessible by 2DIR: (a) quantum beating and is considered. QB pathways inherently pass population transfer, (b) coherence transfer, and (c) population-coherence transfer. The Redfield tensor elements for population transfer and nonsecular relaxation are given above the diagrams for the respective pathways. Dashed lines represent relaxation transitions making up the coherence. between system states.

 $t_3$  CT pathways whose  $\omega_1$  and  $\omega_3$  positions match population transfer diagrams. Such processes also account for line shape distortions by introducing new dynamical processes during the coherence periods. Oscillations in peak intensities are

accounted for by the creation of new quantum representation of various response pathways beating pathways when nonsecular relaxation through a coherence state during the  $t_2$  waiting period,  $^{25,26,46}$  and their intensities along  $t_2$ fluctuate at the difference frequency of the Conveniently, QBs manifest at unique

frequency positions in the rephasing and non-rephasing diagrams under secular conditions. Deviations from this convention then give an experimental indication of nonsecular relaxation. The  $t_1$  CT diagrams in Fig. 1(b) represent coherence transfer pathways which reverse the phase matching dependence of oscillatory peak positions with respect to the secular QBs in Fig. 1(a). The lifetime of CVET pathways is expected to be limited by the dephasing times of the coherences involved, and predominantly contribute to dynamics at early waiting times.<sup>25</sup>

PLEASE CITE THIS ARTICLE AS DOI: 10.1063/5.0216515

While the Feynman diagram representation proves useful for assessing the potential impacts of additional relaxation pathways, the number of possible pathways quickly grows to the point of intractability (further examples given in SI.6). Other works invoke the orientational symmetry requirements of third order response functions<sup>43</sup> to limit the number of relaxation pathways between orthogonal states. <sup>23,24</sup> However, in the case of Fermi coupling, transition dipole moments of the Fermi resonance peak are expected to have significant contributions from the fundamental, <sup>20,39,59,60</sup> and orientational restrictions are relaxed. <sup>46</sup> Marroux et al. proposed a method for eliminating QB pathways and certain coherence transfer pathways by utilizing pump selective experiments. <sup>25</sup> This method makes elimination of Feynman pathways in which the two pump pulses interact with separate oscillators at  $t_1$  and  $t_2$  possible, given sufficient control of the pump bandwidth. Such experiments fully eliminate QBs and reduce the number of nonsecular pathways available to the system. However, nonsecular pathways in which both excitation pulses resonate with a single oscillator still produce peaks in the unpumped regions of these spectra. We leverage this fact to explore complex networks of CVET in our system.

### IV. Results and Discussion

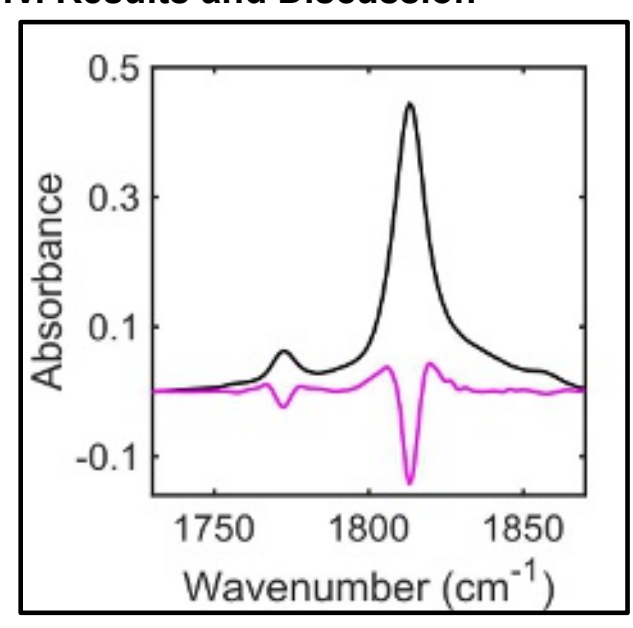


**Fig 2.** Background subtracted FTIR spectrum of EC in THF (black) and corresponding second derivative spectrum (magenta). Second derivative is scaled by a factor of 9.

### A.) Linear IR

The linear IR (black) and second derivative (magenta) spectra of the carbonyl stretching region of EC in THF [Fig. 2] resolve three characteristic bands, 14,16,18 located at 1773 cm<sup>-1</sup>, 1814 cm<sup>-1</sup> and 1858 cm<sup>-1</sup>. The most intense band corresponds to the fundamental of the C=O carbonyl stretch, which is the only fundamental transition expected in the carbonyl region. 16,18 We assume all other bands arise from Fermi resonance couplings with the fundamental and do not consider multiple solvent configurations at this time. Of the two most intense Fermi resonance peaks,

the lower frequency mode at 1773 cm<sup>-1</sup> is assigned to the  $2\nu_7$  overtone of the ring breathing

This is the author's peer reviewed, accepted manuscript. However, the online version of record will be different from this version once it has been copyedited and typeset

PLEASE CITE THIS ARTICLE AS DOI: 10.1063/5.0216515

Between the fundamental and Fermi resonance peaks, the spectrum contains several weaker features which manifest as asymmetry on the high frequency side of the fundamental. Our second derivative spectrum indicates the presence of several additional peaks, which also appear as cross peaks in our 2D spectra. Further discussion of 2DIR cross peaks collected using our full pump bandwidth are given in SI.5. In both linear and nonlinear experiments, the peaks at 1822 cm<sup>-1</sup> and 1828 cm<sup>-1</sup> appear as shoulders to the fundamental transition. Higher frequencies show a broad feature from 1831-1840 cm<sup>-1</sup>. Below the fundamental we observe weak transitions in the range of 1780-1795 cm<sup>-1</sup> as well as a small peak at 1758 cm<sup>-1</sup>. We highlight the 1758 cm<sup>-1</sup> peak due to its proximity to the carbonyl stretching modes of linear carbonates used in conjunction with EC in electrolyte solutions for lithium-ion batteries.<sup>61</sup> While the frequency positions of some of these features overlap with assignments made for solid ethylene carbonate, 16 we do not expect aggregation in our sample based on prior concentration dependent studies. 14,15 However, time dependent linear IR spectra show slight changes in the relative peak intensities of the  $v_2$  and  $2v_7$  bands after four hours, which likely reflect concentration dependent changes due to the evaporation of THF from the sample cell. To avoid the possibility of introducing concentration effects, we limit the acquisition time of our 2DIR experiments.

The linear IR spectrum of EC in THF highlights the congested nature of the carbonyl stretching region. We assume the three largest bands (1773 cm<sup>-1</sup>,1814 cm<sup>-1</sup>,1858 cm<sup>-1</sup>) correspond to the  $2\nu_7, \nu_2$  and  $\nu_6 + \nu_7$  modes. The remaining bands arise from a complex network of Fermi resonance couplings between multi-quanta states and the  $\nu_2$  fundamental transition. We expect that some Fermi resonance bands share common first excited states, as is the case for the  $2\nu_7$  and  $\nu_6 + \nu_7$  bands. Due to the small size and high symmetry of EC this is

PLEASE CITE THIS ARTICLE AS DOI: 10.1063/5.0216515

a safe assumption,<sup>16</sup> and it suggests the possibility of dynamical pathways involving two or more Fermi resonance bands. To experimentally confirm the presence of such pathways and identify the coherent or incoherent nature of vibrational energy transfer in the carbonyl stretching region, we turn to 2DIR.

### B.) Diagonal Bleach: $\nu_2$ and $2\nu_7$

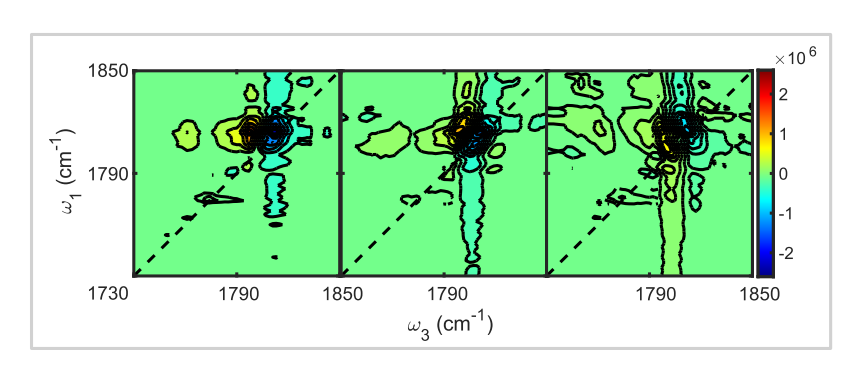


**Fig 3.** Left to right: The purely absorptive, real rephasing, and real non-rephasing 2DIR spectra at  $t_2 = 300$  fs.

In this section we investigate the diagonal features of the  $\nu_2$  (1814 cm<sup>-1</sup>) and  $2\nu_7$  (1773 cm<sup>-1</sup>) transitions. To separate intensity oscillations arising from secular quantum beating

pathways and those arising from nonsecular CVET pathways, we compare the peak dynamics of the purely

absorptive, real rephasing, and real non-rephasing spectra. The rephasing and non-rephasing spectra were extracted from the purely absorptive data by previously outlined methods.<sup>44</sup> The results of this processing are shown in Fig.3. In non-rephasing (rephasing) spectra, secular quantum beats pathways appear as diagonal (cross) peaks. In the absence of CVET, oscillations in the diagonal peak intensities should only appear in the non-rephasing spectrum.

The 2DIR spectra of the  $\nu_2$  and  $2\nu_7$  diagonal peaks are given in Fig. 4(a,d). Blue and red colors correspond to bleach and absorption features, respectively. Fig. 4(a) shows the  $\nu_2$  fundamental bleach at 1814 cm<sup>-1</sup> and its corresponding absorption at 1797cm<sup>-1</sup>, giving an observed diagonal anharmonicity of 17 cm<sup>-1</sup>. The 2D spectrum also reveals an additional shoulder at  $1808 \text{cm}^{-1}$  which was not detected in the linear IR spectrum. We observe several cross peaks involving the fundamental in both the  $\omega_1$  and  $\omega_3$  directions. Slices along each frequency axis are given in SI.5, as well as biexponential fits to the kinetic traces of select cross peaks obtained by integrating a square region of the peak intensities.

This is the author's peer reviewed, accepted manuscript. However, the online version of record will be different from this version once it has been copyedited and typeset PLEASE CITE THIS ARTICLE AS DOI: 10.1063/5.0216515

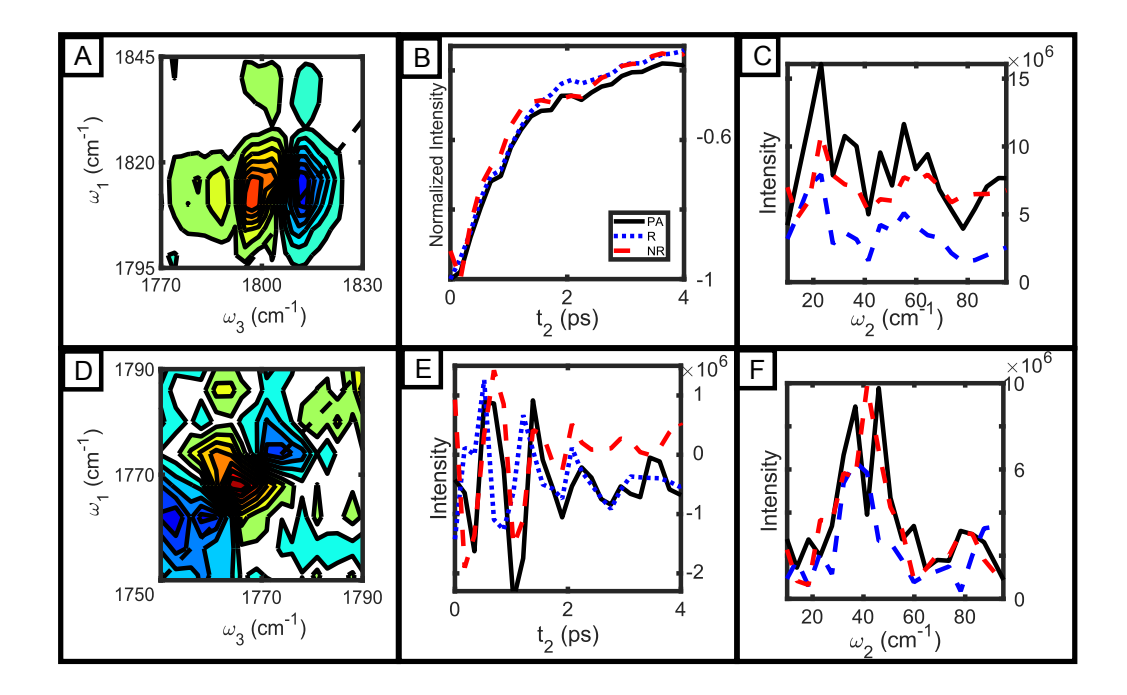


**Fig. 4.** (a) Purely absorptive 2DIR spectrum of the diagonal band of the  $\nu_2$  transition at  $t_2=300$  fs. The color scale ranges from -2.5E7 to 2.5E7 intensity units. (b) Kinetic trace of the diagonal bleach for the purely absorptive (black solid), real rephasing (blue dotted), and real non-rephasing (red dashed) spectra. (c) Absolute value power spectrum obtained by subtracting biexponential fits of the kinetic traces and Fourier-transforming about  $t_2$ . (d) Real non-rephasing spectrum for the diagonal  $2\nu_7$  Fermi resonance peak at  $t_2=100$  fs and color scale -3E6 to 3E6. (e-f) Kinetic trace and power spectrum of diagonal bleach in (d).

To highlight oscillatory features in the  $\nu_2$  diagonal bleach, we plot the self-normalized kinetic traces [Fig. 4(b)] for the purely absorptive (black), real rephasing (blue), and real non-rephasing (red) spectra. Oscillations in the real rephasing spectrum indicate the presence of nonsecular relaxation,<sup>49</sup> although we first address the possibility of beating due to spectral overlap.<sup>26,54</sup> The power spectra, obtained by taking the Fourier transform of the kinetic trace over  $t_2$ , for each phase matching condition [Fig. 4(c)] show beat frequencies to at least 55 cm<sup>-1</sup> which exceeds the approximately 16 cm<sup>-1</sup> Gaussian linewidth obtained from the linear spectrum (see SI.1). In that light congestion seems insufficient to explain the oscillatory dynamics of the fundamental bleach. Additionally, the presence of multiple peaks over a range of frequencies points to CVET pathways involving the fundamental and multiple Fermi resonance peaks.<sup>46</sup>

PLEASE CITE THIS ARTICLE AS DOI: 10.1063/5.0216515

The oscillations in the diagonal peak intensities are clearly present in the  $2v_7$  Fermi resonance peak at 1773 cm<sup>-1</sup>. The non-rephasing spectrum of the  $2\nu_7$  peak at  $t_2$  =100 fs is plotted in Fig. 4(d). As shown by the kinetic trace in Fig. 4(e), this peak manifests predominantly as an oscillation. This likely reflects the low oscillator strength of the Fermi resonance transition compared to that of the fundamental. Based on the ratio of intensities between the two peaks in the linear spectrum (SI.1) and the intensity of the diagonal bleach in Fig.4(a), we estimate that response pathways involving only the  $2\nu_7$  transition would only slightly exceed the noise floor of the experiment. On the contrary, QB pathways involving the stronger  $v_2$  transition should appear with much greater intensity, leading to the observed oscillations in Fig.4(e). It is additionally possible that the low anharmonicity of the underlying ring mode causes annihilation between the excited state absorption and bleach features of traditional response pathways.<sup>62</sup> This further implies that the off-diagonal anharmonicity of the QB pathways exceeds the diagonal anharmonicity associated with the  $2v_7$  mode. Again, oscillations in the real rephasing kinetic trace and corresponding peaks in the power spectrum indicate the 2DIR peak dynamics contain CVET contributions. The rephasing power spectrum in Fig. 4(f) contains peaks with notable intensity at  $\omega_2 = 41 \text{ cm}^{-1}$  (1732 cm<sup>-1</sup>, 1814 cm<sup>-1</sup>) and  $\omega_2 = 85 \text{ cm}^{-1}$  (1688 cm<sup>-1</sup>,1858 cm<sup>-1</sup>), where the values in parentheses are 1773 cm<sup>-1</sup>  $\pm \omega_2$ . The  $+\omega_2$  values coincide exactly with the frequencies of the  $\nu_2$  fundamental transition (1814 cm<sup>-1</sup>) and  $\nu_7 + \nu_6$  Fermi resonance peak (1858 cm<sup>-1</sup>), indicating that CVET processes involving both the fundamental and other Fermi coupled modes contribute to the observed dynamics of the  $2\nu_7$  diagonal feature. As we detect neither evidence of vibrational ladder climbing<sup>24,63,64</sup> (SI.7) nor accidental peak overlap<sup>65</sup> (SI.8), we consider the dynamics observed in Fig.4(b,e) to reflect genuine CVET pathways between vibrational resonance states in EC.

CVET contributions also appear in the observed frequency-frequency correlation function (FFCF) of the  $\nu_2$  diagonal bleach. The normalized FFCF, denoted by  $\bar{C}(t_2)$ , for the  $\nu_2$ band is given on the left-hand side of Fig. 5. We obtain the FFCF by means of the inhomogeneity index,45,66 defined by:

$$II(t_2) = \frac{A_R(t_2) - A_{NR}(t_2)}{A_R(t_2) + A_{NR}(t_2)} \tag{2}$$

and

$$\bar{C}(t_2) = \sin\left(\frac{\pi}{2} \times II\right). \tag{3}$$

PLEASE CITE THIS ARTICLE AS DOI: 10.1063/5.0216515

Here  $A_R$  and  $A_{NR}$  give the integrated intensity of the absolute value of the rephasing and non-rephasing spectra for a region of interest. We assess the contribution of noise by

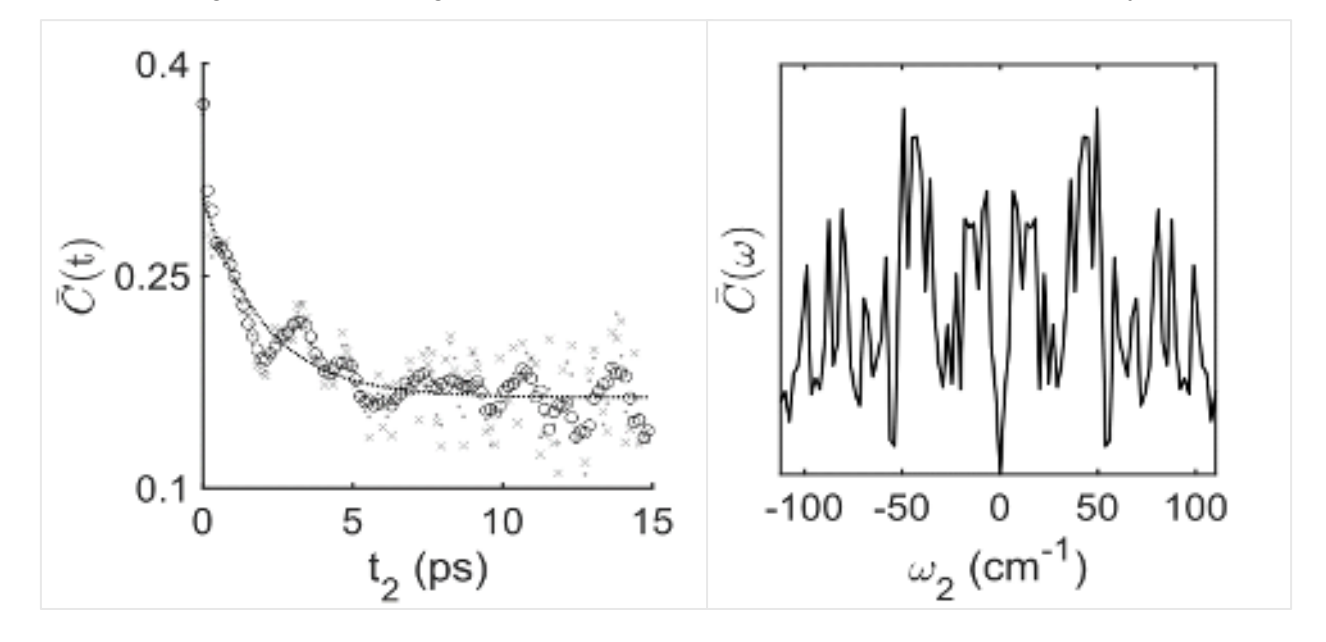


**Fig. 5. Left:** The normalized frequency-frequency correlation function for the fundamental bleach obtained by inhomogeneity index. Scatter plots are given for rephasing and non-rephasing intensities treated with a moving average (circles), Savitzky–Golay (dot), and no filter (x). The dashed line gives the mono-exponential fit of the dotted line. **Right:** Normalized power spectral density obtained by subtracting the fit from the FFCF and Fourier-transforming about the waiting time.

comparing the experimental FFCF when treating rephasing and non-rephasing intensities with different noise filters. The scatter plots in Fig. 5 correspond to a moving average filter (circles), Savitzky-Golay filter (x's), or no noise filter (dots). As all three data sets show similar oscillatory character out to 5 ps, we take this as the upper limit for experimentally resolving oscillations from noise. We fit  $\bar{C}(t_2)$  to the form  $ae^{\frac{-t_2}{\tau_{corr}}} + c$ , yielding  $\tau_{corr} = 2.05 \pm 0.36$  ps. In the absence of strong coupling,  $\tau_{corr}$  provides an approximate upper bound to the timescales of CVET involving the state  $|\nu_2\rangle$  (0| or its complex conjugate. Both the kinetic traces in Fig. 4(b,e) and the FFCF in Fig. 5 oscillate at times later than  $\tau_{corr}$ , suggesting an extension of coherence lifetimes due to the coupling of coherences with elements of the system and/or bath.

The coupling of the system to low frequency bath modes may give rise to the oscillations of the FFCF. Such assignments have been made previously for time dependent vibrational studies of hydrogen bonding in water.<sup>67–69</sup> To assess the character of the oscillations, we investigate the spectral density  $\bar{C}(\omega)$ , obtained by subtracting the exponential component of  $\bar{C}(t_2)$  and taking the Fourier transform of  $\bar{C}(t_2)$ . Those results are given on the right-hand side

This is the author's peer reviewed, accepted manuscript. However, the online version of record will be different from this version once it has been copyedited and typeset

PLEASE CITE THIS ARTICLE AS DOI: 10.1063/5.0216515

In the context of nonsecular relaxation between system states, such oscillations may arise from CVET processes during the  $t_2$  waiting period. In this interpretation the timescales of the oscillations reflect either the dephasing times of coherences involving multiple excited states, or the lifetimes of populations coupled to coherence states. As we do not detect a dampening of the oscillations in  $\bar{C}(t_2)$  before the onset of noise, we cannot use timescales to distinguish these effects directly. Instead, we estimate them from the quantum beating character of the  $2v_7$ diagonal feature. The integrated intensity of the fits to the linear spectrum yields an approximately 3:1 transition dipole strength ratio for the  $v_2$  and  $2v_7$  band. We expect the decay of the diagonal feature of the  $2v_7$  band predominantly describes the dephasing of the coherence state  $|\nu_2\rangle\langle 2\nu_7|$ , as coherences between Fermi resonance states contribute only weakly.

To obtain dynamical data on the Fermi resonance band we follow the method of Roberts et al.66 The relaxation is calculated according to:

$$A_R + A_{NR} = \frac{\pi}{\langle \delta \omega^2 \rangle \sqrt{1 - \bar{C}(t_2)^2}} e^{\frac{-t_2}{T_1}} \tag{4}$$

where  $T_1$  is the vibrational relaxation and  $\delta\omega$  is the fluctuation amplitude. <sup>39,71</sup> Rearranging this equation allows one to solve for  $T_1$  while avoiding destructive interference between the rephasing and non-rephasing pathways. We test this method using the  $\nu_2$  diagonal bleach for which we obtain a biexponential decay with time constants of  $T_1^{fast} = 1.39 \pm 0.3$  ps and  $T_1^{slow} =$ 14.92 ± 0.31 ps. We compare these fits to values obtained by fitting the kinetic trace of the purely absorptive spectrum and find excellent agreement (see SI.5). We then apply this metric to the  $2\nu_7$  diagonal band, giving a singular exponential decay with time constant  $T_1 = 0.94 \pm$ 0.29 ps. Given that this feature appears as a quantum beat, it is not clear that this truly reflects

This is the author's peer reviewed, accepted manuscript. However, the online version of record will be different from this version once it has been copyedited and typeset

### C.) Pump selective 2DIR

In this section we consider the positions and intensities of bandwidth forbidden cross peaks appearing in the unpumped regions of the pump selective spectra presented in Fig. 6. These peaks provide an additional experimental check for the presence of CVET. In a Feynman diagram picture one can imagine such peaks arising from responses of the form:

in which the transition from the ground state to  $\alpha$  lies within the pump bandwidth and the ground state to β transition does not. Under these conditions no secular response pathways produce features at  $\omega_1 = \omega_{\beta,0}$ . This provides an intuitive picture by which the surviving nonsecular pathways contain character of both the allowed and bandwidth forbidden transitions over  $t_1$ , and therefore contribute to the unpumped region of the spectrum. While the Feynman diagram representation is not exact, we do find experimental evidence that forbidden cross peaks on the  $\omega_1$  axis correspond to coherence transfer occurring over the  $t_1$  interval. In SI.4 we compare the dynamics of the same cross peak under fully pumped (ordinary) and pump selective (forbidden) conditions. We treat the time domain data with varying window functions

the online version of record will be different from this version once it has been copyedited and typeset This is the author's peer reviewed, accepted manuscript. However,

PLEASE CITE THIS ARTICLE AS DOI: 10.1063/5.0216515

The vertically plotted spectra of the righthand side of Fig. 6 give the normalized pump spectrum for each pump selective 2DIR experiment (left). The red dashed lines indicate the region in which the pump intensity falls below 10% of the maximum, and we consider features in this region to be bandwidth forbidden. The forbidden region of each spectrum is highlighted with a blue/grey background. We describe cross peaks in the fully pumped spectra as ordinary cross peaks. The frequency cutoffs of the pump pulses in Fig. 6(a-d) are:  $\omega_{pump}$ >1795 cm<sup>-1</sup>,  $\omega_{pump}{>}1816~\mathrm{cm^{-1}}$  ,  $\omega_{pump}{<}1831~\mathrm{cm^{-1}}$  , and  $\omega_{pump}{<}1815$ cm<sup>-1</sup>. The linear IR spectrum is plotted above for convenience. Only the experiment in which the  $v_2$ fundamental transition (1814 cm<sup>-1</sup>) lies outside the pump frequency [Fig. 6(b)] fails to resolve forbidden peaks, likely due to blocking the strong  $v_2$  fundamental transition. We focus our analysis on the bandwidth forbidden peaks appearing at the detection frequency of the  $\nu_2$ fundamental. The number of anomalous peaks and the range over which they appear along  $\omega_1$  in Fig. 6 suggests CVET pathways disperse vibrational energy over many different overtone and combination states of low frequency modes. The observation of these forbidden peaks is significant, in that single coherence transfer pathways have been omitted in other studies investigating nonsecular relaxation in 2DIR, on the basis of transition dipole moment orthogonality in the corresponding model system.<sup>25,26</sup> The spectral signatures of single coherence transfer are thus not well

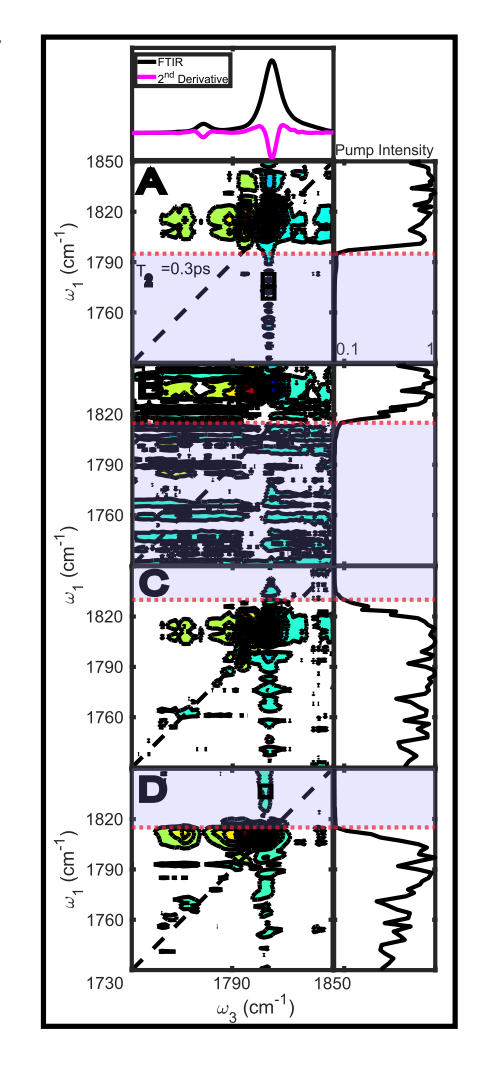


Fig 6. Right: normalized pump spectrum for each pump selective 2DIR experiment. Left: Pump selective 2DIR spectra at  $t_2 = 300$ fs. The red dashed lines indicate the  $\omega_1$  frequency at which features are considered forbidden, and the forbidden regions are marked by a blue/grey background. Black squares indicate cross peaks discussed in Fig. 7. The pump frequency cutoffs and color scale for each experiment are: (a)  $\omega_{pump}$ >1795 cm<sup>-1</sup> (±3E6) ,(**b**)  $\omega_{pump}$  >1816 cm<sup>-1</sup> (±2.5E5), (**c**)  $\omega_{vumv}$ <1831 cm<sup>-1</sup> (±2.3E6), and (**d**).  $\omega_{numn}$ <1815 cm<sup>-1</sup> (±1.8E6).

This is the author's peer reviewed, accepted manuscript. However, the online version of record will be different from this version once it has been copyedited and typeset

PLEASE CITE THIS ARTICLE AS DOI: 10.1063/5.0216515

characterized. This makes EC a strong candidate for theoretical investigations which may provide additional insight for interpreting coherence transfer in 2DIR spectra.

One alternative explanation for the range of forbidden peaks is incomplete cancellation between rephasing and non-rephasing pathways, resulting in phase twist.<sup>25,26</sup> This may arise from both secular and nonsecular quantum beating pathways and leads to distortions in the absorptive spectrum. If this is the origin of the forbidden peaks, their intensity should decay according to coherence dephasing rather than population lifetimes.<sup>28</sup> One would then expect the

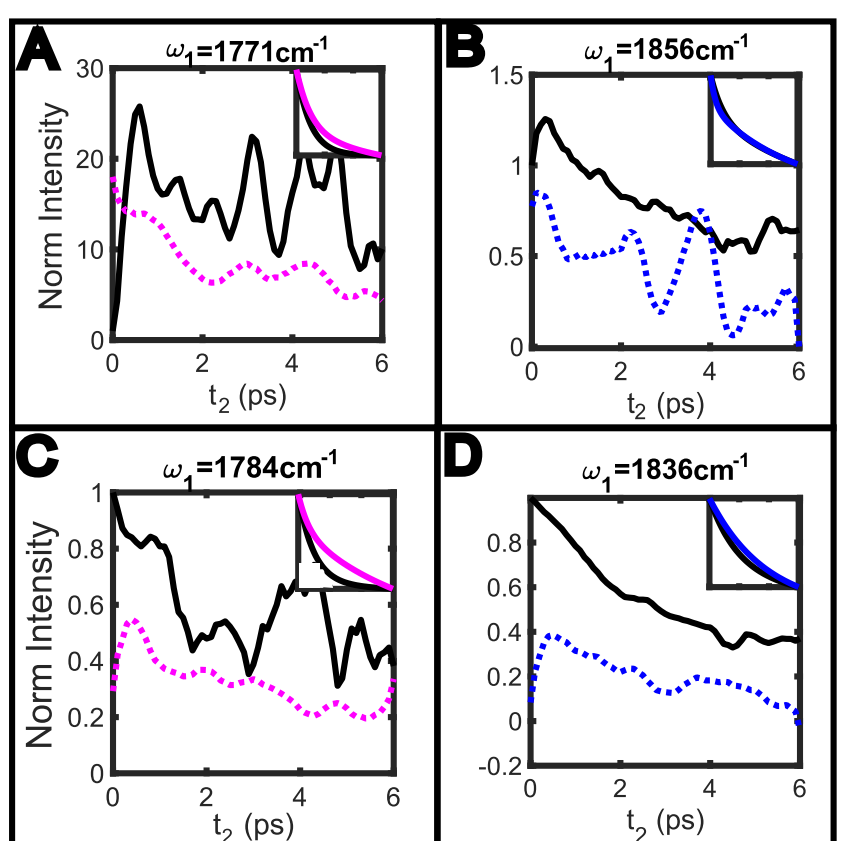


Fig 7. Comparing kinetic traces for bandwidth forbidden cross peaks (dotted lines) to their ordinary cross peak (solid black). Both intensities are normalized to the fully pumped intensity at zero waiting time. (a,c) taken from pump selective experiment  $\omega_{pump} > 1795~{\rm cm}^{-1}$ . (b,d) taken from pump selective experiment  $\omega_{pump} < 1815~{\rm cm}^{-1}$ . Inset of each figure gives the normalized biexponential fit of the decay component of the integrated intensities. All kinetic traces were treated with a moving average filter to suppress high frequency noise.

forbidden peaks to decay more rapidly during the waiting period. We fit the kinetic trace of four cross peaks to biexponential decays. The normalized fits to the intensity of forbidden pump-selective (colored) and ordinary full-pump (black) spectra are presented as insets of Fig. 7. The  $\omega_1$ position of the cross peak is given above each plot. From the fits in Fig. 7, we see that the forbidden peaks and the corresponding fully pumped cross peaks share similar  $t_2$ 

dynamics and are therefore unlikely to be the result of incomplete cancellation between the rephasing and non-rephasing pathways. The observation that the bandwidth forbidden peaks in Fig. 7(a,c,d) have somewhat slower decays could suggest that ordinary pathways passing through a Fermi resonance

PLEASE CITE THIS ARTICLE AS DOI: 10.1063/5.0216515

population during  $t_2$  are subject to rapid relaxation, while CVET pathways involving  $t_2$  coherences decay more slowly due to coupling with population states.

Next, we assess the potential impacts of CVET on interpretation of cross peak intensities. In the main portion of Fig. 7, we plot the ordinary and bandwidth forbidden cross peaks normalized to the initial intensity of the ordinary cross peak. Fig. 7(a,b) correspond to cross peaks between the fundamental and two most intense Fermi resonance bands  $(2v_7, v_6 +$  $v_7$ ) in the linear spectrum. Both show an initial growth in the fully pumped spectrum, indicating rapid vibrational energy transfer between the Fermi resonance modes and the  $\nu_2$  fundamental. Based on the  $\omega_1$  position of the cross peaks, growths in the kinetic trace could be interpreted as energy transfer from the Fermi resonance modes into the fundamental; however, a similar growth appears for the  $v_6 + v_7$  bandwidth forbidden kinetic trace [Fig. 7(b)]. This indicates that the growth is not due to population transfer into  $v_2$ , but rather it reflects CVET from the fundamental into  $\nu_6 + \nu_7$ . As such the dynamics could be significantly misinterpreted in the secular approximation. The bandwidth forbidden kinetic trace of the  $2\nu_7$  cross peak [Fig. 7(a)] presents even more interesting dynamics, in that the initial intensity appears greater in the absence of direct excitation. This defies conventional wisdom, and we cannot offer a satisfactory explanation. Such results may reflect complicated relaxation processes involving multiple steps. Conversely, the cross peaks represented in Fig. 7(c,d) clearly show an initial growth only for forbidden peaks. In the case of Fig. 7(c), it appears this growth interferes with additional oscillatory components. This suggests the possibility of interference between secular quantum beating and potentially many CVET processes. If oscillatory processes contain phase offsets or different frequency components, neither may be directly resolvable by experiment. In Fig. 7(d) the coherent growth appears masked by additional incoherent relaxation mechanisms present in the ordinary cross peak. Taken together these dynamics indicate a complex relationship between CVET, population dynamics, and secular quantum beating which need to be accounted for to extract accurate dynamics from 2DIR spectra.

From these experiments we also obtain some insight on the relative strength of CVET processes contributing to different peaks. Khalil et al. demonstrated the intensity of forbidden peaks at  $t_2=0$  is proportional to the nonsecular transfer rate. Applying this result to our pump selective experiments, we express the initial intensity of the forbidden cross peak as a percentage of the initial intensity of the ordinary cross peak. This metric gives an estimate of CVET character of the early time dynamics of each cross peak. We apply this metric to the kinetic traces in Fig. 7 to assess the strength of nonsecular relaxation for the cross peaks in Fig.

# This is the author's peer reviewed, accepted manuscript. However, the online version of record will be different from this version once it has been copyedited and typeset PLEASE CITE THIS ARTICLE AS DOI: 10.1063/5.0216515

7(b-d). We do not interpret this value for Fig. 7(a), as competing effects clearly need consideration. The other peaks behave as expected, although the peaks in Fig. 7(b) and Fig. 7(c) show significant CVET contributions which make up 77% and 29% of the zero waiting time intensities, respectively. The peak in Fig. 7(d) indicates the weakest CVET character, with only 8% of its early waiting time intensity present in the pump selective data. It is interesting that the strongest Fermi resonance bands in the linear spectrum also show the greatest CVET character, although we cannot say if this indicates a more significant relationship or is simply a coincidence. Isotope labeling or solvent variational 2DIR experiments may serve to clarify the cause and nature of CVET in ethylene carbonate. The degree to which CVET presents itself in other Fermi coupled systems can be assessed by time dependent vibrational studies which focus on identifying coherent dynamics.

### **V. Conclusion**

From the linear IR spectrum, we observe that the carbonyl region of EC in THF represents a complex vibrational landscape containing multiple Fermi resonance peaks and a single fundamental transition. Immediately upon investigating the diagonal dynamics of the  $\nu_2$  fundamental we find evidence of coherent dynamics in the form of multiple oscillations in the real rephasing kinetic trace. The power spectrum of the oscillations in the kinetic trace suggests the coherent dynamics reflect coupling of the fundamental and several Fermi resonance modes. The diagonal bleach of the  $2\nu_7$  Fermi resonance peak appears entirely as an oscillation and its power spectrum reveals CVET not only with the fundamental but also amongst Fermi resonance bands. We find the coherence lifetimes of the  $\nu_2$  and  $2\nu_7$  diagonal peaks shorter than the timescale of coherent oscillations in the spectrum. We take this to indicate that the long-lived oscillations arise from coupling between coherence and population states.

We then confirm the presence of single coherence transfer pathways with pump selective 2DIR experiments. In those experiments we observe bandwidth forbidden peaks in the unpumped region of the spectrum, indicating single coherence transfer processes. As such it could serve as a system against which to test more general models of coherent dynamics. Upon investigating the relative intensities of unpumped cross peaks, we observe that several cross peaks contain significant contributions from CVET, with the cross peak corresponding to the  $2\nu_7$  band appearing more strongly when it lies outside the pump bandwidth. We find that the growth of forbidden cross peaks obscures the nature of vibrational dynamics in the system. The dynamics of forbidden peaks reflect a complex interplay of coherent and incoherent dynamics

PLEASE CITE THIS ARTICLE AS DOI: 10.1063/5.0216515

which must be carefully considered to extract accurate dynamical information from experiments. Future work will be needed to characterize these coherent dynamics and assess their information content, so that we can better utilize molecules like EC as vibrational probes.

### **ACKNOWLEDGEMENTS**

This work was supported by the National Science Foundation under Award No.2108346.

### **Supplementary Material**

See supplementary material for: fitting of linear spectrum, characterization of noise in 2DIR spectra, comparison of diagonal peak intensities for ordinary and pump selective 2DIR experiments, characterization of the  $t_1$  scan dependence of ordinary and forbidden cross peak, fits to the integrated intensities of diagonal and cross peaks under ordinary conditions, select Feynman diagrams for nonsecular relaxation pathways considered in this work, considerations of vibrational ladder climbing pathways, and coherence maps for the real rephasing spectrum at  $\omega_2 = 41 \text{ cm}^{-1}$ .

### **Author Declaration**

The authors have no conflicts to disclose.

### **Author Contributions**

**Luke Guerrieri:** Conceptualization; Data curation; Formal analysis; Investigation; Methodology; Visualization; Writing- original draft. **Sarah Hall:** Investigation; Methodology; Writing-reviewing and editing. **Brad M. Luther:** Methodology; Writing-reviewing and editing. **Amber T. Krummel:** Conceptualization; Funding acquisition; Resources; Writing- reviewing and editing.

**Corresponding Author**: Amber T. Krummel

### **Data Availability**

## the online version of record will be different from this version once it has been copyedited and typeset accepted manuscript. However, This is the author's peer reviewed,

PLEASE CITE THIS ARTICLE AS DOI: 10.1063/5.0216515

The data that support the findings of this study are available from the corresponding author upon reasonable request

### References

- (1) Galle Kankanamge, S. R.; Kuroda, D. G. Molecular Structure, Chemical Exchange, and Conductivity Mechanism of High Concentration LiTFSI Electrolytes. *J. Phys. Chem. B* **2020**, *124* (10), 1965–1977. https://doi.org/10.1021/acs.jpcb.9b10795.
- (2) Fulfer, K. D.; Kuroda, D. G. Solvation Structure and Dynamics of the Lithium Ion in Organic Carbonate-Based Electrolytes: A Time-Dependent Infrared Spectroscopy Study. *J. Phys. Chem. C* **2016**, *120* (42), 24011–24022. https://doi.org/10.1021/acs.jpcc.6b08607.
- (3) Fulfer, K. D.; Kuroda, D. G. Ion Speciation of Lithium Hexafluorophosphate in Dimethyl Carbonate Solutions: An Infrared Spectroscopy Study. *Phys. Chem. Chem. Phys.* **2018**, *20* (35), 22710–22718. https://doi.org/10.1039/C8CP03315C.
- (4) Fulfer, K. D.; Galle Kankanamge, S. R.; Chen, X.; Woodard, K. T.; Kuroda, D. G. Elucidating the Mechanism behind the Infrared Spectral Features and Dynamics Observed in the Carbonyl Stretch Region of Organic Carbonates Interacting with Lithium Ions. *J. Chem. Phys.* **2021**, *154* (23), 234504. https://doi.org/10.1063/5.0049742.
- (5) Tale of a "Non-interacting" Additive in a Lithium-Ion Electrolyte: Effect on Ionic Speciation and Electrochemical Properties | The Journal of Physical Chemistry C. https://pubs.acs.org/doi/10.1021/acs.jpcc.1c09193 (accessed 2024-03-12).
- (6) Dereka, B.; Lewis, N. H. C.; Zhang, Y.; Hahn, N. T.; Keim, J. H.; Snyder, S. A.; Maginn, E. J.; Tokmakoff, A. Exchange-Mediated Transport in Battery Electrolytes: Ultrafast or Ultraslow? *J. Am. Chem. Soc.* **2022**, *144* (19), 8591–8604. https://doi.org/10.1021/jacs.2c00154.
- (7) Fulfer, K. D.; Kuroda, D. G. A Comparison of the Solvation Structure and Dynamics of the Lithium Ion in Linear Organic Carbonates with Different Alkyl Chain Lengths. *Phys. Chem. Chem. Phys.* **2017**, *19* (36), 25140–25150. https://doi.org/10.1039/C7CP05096H.
- (8) Liang, C.; Kwak, K.; Cho, M. Revealing the Solvation Structure and Dynamics of Carbonate Electrolytes in Lithium-Ion Batteries by Two-Dimensional Infrared Spectrum Modeling. *J. Phys. Chem. Lett.* **2017**, *8* (23), 5779–5784. https://doi.org/10.1021/acs.jpclett.7b02623.

# the online version of record will be different from this version once it has been copyedited and typeset This is the author's peer reviewed, accepted manuscript. However,

PLEASE CITE THIS ARTICLE AS DOI: 10.1063/5.0216515

- (9) Lim, C.; Kim, J. H.; Chae, Y.; Lee, K.-K.; Kwak, K.; Cho, M. Solvation Structure around Li+ Ions in Organic Carbonate Electrolytes: Spacer-Free Thin Cell IR Spectroscopy. *Anal. Chem.* **2021**, 93 (37), 12594–12601. https://doi.org/10.1021/acs.analchem.1c02127.
- (10) Two-Dimensional Infrared Spectroscopy and Molecular Dynamics Simulation Studies of Nonaqueous Lithium Ion Battery Electrolytes | The Journal of Physical Chemistry B. https://pubs.acs.org/doi/10.1021/acs.jpcb.9b02026 (accessed 2024-03-12).
- (11) Effect of Solvation Shell Structure and Composition on Ion Pair Formation: The Case Study of LiTDI in Organic Carbonates | The Journal of Physical Chemistry C. https://pubs.acs.org/doi/10.1021/acs.jpcc.9b07469 (accessed 2024-03-12).
- (12) Zhang, X.; Kuroda, D. G. An Ab Initio Molecular Dynamics Study of the Solvation Structure and Ultrafast Dynamics of Lithium Salts in Organic Carbonates: A Comparison between Linear and Cyclic Carbonates. *J. Chem. Phys.* **2019**, *150* (18), 184501. https://doi.org/10.1063/1.5088820.
- (13) Jiang, B.; Ponnuchamy, V.; Shen, Y.; Yang, X.; Yuan, K.; Vetere, V.; Mossa, S.; Skarmoutsos, I.; Zhang, Y.; Zheng, J. The Anion Effect on Li+ Ion Coordination Structure in Ethylene Carbonate Solutions. *J. Phys. Chem. Lett.* **2016**, *7* (18), 3554–3559. https://doi.org/10.1021/acs.jpclett.6b01664.
- (14) Fini, G.; Mirone, P.; Fortunato, B. Evidence for Short-Range Orientation Effects in Dipolar Aprotic Liquids from Vibrational Spectroscopy. Part 1.—Ethylene and Propylene Carbonates. *J. Chem. Soc. Faraday Trans. 2 Mol. Chem. Phys.* **1973**, 69 (0), 1243–1248. https://doi.org/10.1039/F29736901243.
- (15) Schindler, W.; Zerda, T. W.; Jonas, J. High Pressure Raman Study of Intermolecular Interactions and Fermi Resonance in Liquid Ethylene Carbonate. *J. Chem. Phys.* **1984**, *81* (10), 4306–4313. https://doi.org/10.1063/1.447440.
- (16) Fortunato, B.; Mirone, P.; Fini, G. Infrared and Raman Spectra and Vibrational Assignment of Ethylene Carbonate. *Spectrochim. Acta Part Mol. Spectrosc.* **1971**, *27* (9), 1917–1927. https://doi.org/10.1016/0584-8539(71)80245-3.
- (17) Klassen, B.; Aroca, R.; Nazri, M.; Nazri, G. A. Raman Spectra and Transport Properties of Lithium Perchlorate in Ethylene Carbonate Based Binary Solvent Systems for Lithium Batteries. *J. Phys. Chem. B* **1998**, *102* (24), 4795–4801. https://doi.org/10.1021/jp973099d.
- (18) Bertran, J. F.; Ballester, L.; Dobrihalova, L.; Sánchez, N.; Arrieta, R. Study of Fermi Resonance by the Method of Solvent Variation. *Spectrochim. Acta Part Mol. Spectrosc.* **1968**, *24* (11), 1765–1776. https://doi.org/10.1016/0584-8539(68)80232-6.
- (19) Zhang, J.; Wang, L.; Zhang, J.; Zhu, J.; Pan, X.; Cui, Z.; Wang, J.; Fang, W.; Li, Y. Identifying and Modulating Accidental Fermi Resonance: 2D IR and DFT Study of 4-Azido-l-Phenylalanine. *J. Phys. Chem. B* **2018**, *122* (34), 8122–8133. https://doi.org/10.1021/acs.jpcb.8b03887.
- (20) Park, J. Y.; Mondal, S.; Kwon, H.-J.; Sahu, P. K.; Han, H.; Kwak, K.; Cho, M. Effect of Isotope Substitution on the Fermi Resonance and Vibrational Lifetime of Unnatural Amino Acids Modified

. However, the online version of record will be different from this version once it has been copyedited and typeset. PLEASE CITE THIS ARTICLE AS DOI: 10.1063/5.0216515 This is the author's peer reviewed, accepted manuscript. However,

- (21) Heyne, K.; Huse, N.; Dreyer, J.; Nibbering, E. T. J.; Elsaesser, T.; Mukamel, S. Coherent Low-Frequency Motions of Hydrogen Bonded Acetic Acid Dimers in the Liquid Phase. *J. Chem. Phys.* **2004**, *121* (2), 902–913. https://doi.org/10.1063/1.1762873.
- (22) Gündoğdu, K.; Bandaria, J.; Nydegger, M.; Rock, W.; Cheatum, C. M. Relaxation and Anharmonic Couplings of the O–H Stretching Vibration of Asymmetric Strongly Hydrogen-Bonded Complexes. *J. Chem. Phys.* **2007**, *127* (4), 044501. https://doi.org/10.1063/1.2753840.
- (23) Baiz, C. R.; Kubarych, K. J.; Geva, E. Molecular Theory and Simulation of Coherence Transfer in Metal Carbonyls and Its Signature on Multidimensional Infrared Spectra. *J. Phys. Chem. B* **2011**, *115* (18), 5322–5339. https://doi.org/10.1021/jp109357d.
- (24) Eckert, P. A.; Kubarych, K. J. Vibrational Coherence Transfer Illuminates Dark Modes in Models of the FeFe Hydrogenase Active Site. *J. Chem. Phys.* **2019**, *151* (5), 054307. https://doi.org/10.1063/1.5111016.
- (25) Marroux, H. J. B.; Orr-Ewing, A. J. Distinguishing Population and Coherence Transfer Pathways in a Metal Dicarbonyl Complex Using Pulse-Shaped Two-Dimensional Infrared Spectroscopy. *J. Phys. Chem. B* **2016**, *120* (17), 4125–4130. https://doi.org/10.1021/acs.jpcb.6b02979.
- (26) Khalil, M.; Demirdöven, N.; Tokmakoff, A. Vibrational Coherence Transfer Characterized with Fourier-Transform 2D IR Spectroscopy. *J. Chem. Phys.* **2004**, *121* (1), 362–373. https://doi.org/10.1063/1.1756870.
- (27) Redfield, A. G. The Theory of Relaxation Processes\*. In *Advances in Magnetic and Optical Resonance*; Waugh, J. S., Ed.; Advances in Magnetic Resonance; Academic Press, 1965; Vol. 1, pp 1–32. https://doi.org/10.1016/B978-1-4832-3114-3.50007-6.
- (28) Chang, T.-M.; Skinner, J. L. Non-Markovian Population and Phase Relaxation and Absorption Lineshape for a Two-Level System Strongly Coupled to a Harmonic Quantum Bath. *Phys. Stat. Mech. Its Appl.* **1993**, *193* (3), 483–539. https://doi.org/10.1016/0378-4371(93)90489-Q.
- (29) Eastham, P. R.; Kirton, P.; Cammack, H. M.; Lovett, B. W.; Keeling, J. Bath-Induced Coherence and the Secular Approximation. *Phys. Rev. A* **2016**, 94 (1), 012110. https://doi.org/10.1103/PhysRevA.94.012110.
- (30) Jeske, J.; Ing, D. J.; Plenio, M. B.; Huelga, S. F.; Cole, J. H. Bloch-Redfield Equations for Modeling Light-Harvesting Complexes. *J. Chem. Phys.* **2015**, *142* (6), 064104. https://doi.org/10.1063/1.4907370.
- (31) Balzer, B.; Stock, G. Modeling of Decoherence and Dissipation in Nonadiabatic Photoreactions by an Effective-Scaling Nonsecular Redfield Algorithm. *Chem. Phys.* **2005**, *310* (1), 33–41. https://doi.org/10.1016/j.chemphys.2004.10.001.

# . However, the online version of record will be different from this version once it has been copyedited and typeset. PLEASE CITE THIS ARTICLE AS DOI: 10.1063/5.0216515 This is the author's peer reviewed, accepted manuscript. However,

- (32) Ishizaki, A.; Fleming, G. R. On the Adequacy of the Redfield Equation and Related Approaches to the Study of Quantum Dynamics in Electronic Energy Transfer. *J. Chem. Phys.* **2009**, *130* (23), 234110. https://doi.org/10.1063/1.3155214.
- (33) Engel, G. S.; Calhoun, T. R.; Read, E. L.; Ahn, T.-K.; Mančal, T.; Cheng, Y.-C.; Blankenship, R. E.; Fleming, G. R. Evidence for Wavelike Energy Transfer through Quantum Coherence in Photosynthetic Systems. *Nature* **2007**, *446* (7137), 782–786. https://doi.org/10.1038/nature05678.
- (34) Hidden vibronic and excitonic structure and vibronic coherence transfer in the bacterial reaction center. https://doi.org/10.1126/sciadv.abk0953.
- (35) Luther, B. M.; Tracy, K. M.; Gerrity, M.; Brown, S.; Krummel, A. T. 2D IR Spectroscopy at 100 kHz Utilizing a Mid-IR OPCPA Laser Source. *Opt. Express* **2016**, *24* (4), 4117–4127. https://doi.org/10.1364/OE.24.004117.
- (36) Luther, B. M.; Tracy, K. M.; Krummel, A. T. Demonstrating 100 kHz 2D IR Spectroscopy Using a Mid-IR OPCPA Laser Source. In *International Conference on Ultrafast Phenomena (2016), paper UTu2A.5*; Optica Publishing Group, 2016; p UTu2A.5. https://doi.org/10.1364/UP.2016.UTu2A.5.
- (37) Guchhait, B.; Tibbetts, C. A.; Tracy, K. M.; Luther, B. M.; Krummel, A. T. Ultrafast Vibrational Dynamics of a Trigonal Planar Anionic Probe in Ionic Liquids (ILs): A Two-Dimensional Infrared (2DIR) Spectroscopic Investigation. *J. Chem. Phys.* **2020**, *152* (16), 164501. https://doi.org/10.1063/1.5141751.
- (38) Shim, S.-H.; Zanni, M. T. How to Turn Your Pump–Probe Instrument into a Multidimensional Spectrometer: 2D IR and Vis Spectroscopiesvia Pulse Shaping. *Phys. Chem. Chem. Phys.* **2009**, *11* (5), 748–761. https://doi.org/10.1039/B813817F.
- (39) Hamm, P.; Zanni, M. *Concepts and Methods of 2D Infrared Spectroscopy*; Cambridge University Press: Cambridge, 2011. https://doi.org/10.1017/CBO9780511675935.
- (40) Nishida, J.; Tamimi, A.; Fei, H.; Pullen, S.; Ott, S.; Cohen, S. M.; Fayer, M. D. Structural Dynamics inside a Functionalized Metal–Organic Framework Probed by Ultrafast 2D IR Spectroscopy. *Proc. Natl. Acad. Sci. U. S. A.* **2014**, *111* (52), 18442–18447. https://doi.org/10.1073/pnas.1422194112.
- (41) Feng, Y.; Vinogradov, I.; Ge, N.-H. General Noise Suppression Scheme with Reference Detection in Heterodyne Nonlinear Spectroscopy. *Opt. Express* **2017**, *25* (21), 26262–26279. https://doi.org/10.1364/OE.25.026262.
- (42) Feng, Y.; Vinogradov, I.; Ge, N.-H. Optimized Noise Reduction Scheme for Heterodyne Spectroscopy Using Array Detectors. *Opt. Express* **2019**, *27* (15), 20323–20346. https://doi.org/10.1364/OE.27.020323.
- (43) Hochstrasser, R. M. Two-Dimensional IR-Spectroscopy: Polarization Anisotropy Effects. *Chem. Phys.* **2001**, 266 (2), 273–284. https://doi.org/10.1016/S0301-0104(01)00232-4.
- (44) Zhang, Z.; Wells, K. L.; Hyland, E. W. J.; Tan, H.-S. Phase-Cycling Schemes for Pump–Probe Beam Geometry Two-Dimensional Electronic Spectroscopy. *Chem. Phys. Lett.* **2012**, *550*, 156–161. https://doi.org/10.1016/j.cplett.2012.08.037.

# the online version of record will be different from this version once it has been copyedited and typeset This is the author's peer reviewed, accepted manuscript. However,

PLEASE CITE THIS ARTICLE AS DOI: 10.1063/5.0216515

- (45) Duan, R.; Mastron, J. N.; Song, Y.; Kubarych, K. J. Direct Comparison of Amplitude and Geometric Measures of Spectral Inhomogeneity Using Phase-Cycled 2D-IR Spectroscopy. *J. Chem. Phys.* **2021**, *154* (17), 174202. https://doi.org/10.1063/5.0043961.
- (46) Nee, M. J.; Baiz, C. R.; Anna, J. M.; McCanne, R.; Kubarych, K. J. Multilevel Vibrational Coherence Transfer and Wavepacket Dynamics Probed with Multidimensional IR Spectroscopy. *J. Chem. Phys.* **2008**, *129* (8), 084503. https://doi.org/10.1063/1.2969900.
- (47) Manzano, D. A Short Introduction to the Lindblad Master Equation. *AIP Adv.* **2020**, *10* (2), 025106. https://doi.org/10.1063/1.5115323.
- (48) Montoya-Castillo, A.; Berkelbach, T. C.; Reichman, D. R. Extending the Applicability of Redfield Theories into Highly Non-Markovian Regimes. *J. Chem. Phys.* **2015**, *143* (19), 194108. https://doi.org/10.1063/1.4935443.
- (49) Abramavicius, D.; Mukamel, S. Quantum Oscillatory Exciton Migration in Photosynthetic Reaction Centers. *J. Chem. Phys.* **2010**, *133* (6), 064510. https://doi.org/10.1063/1.3458824.
- (50) Palmieri, B.; Abramavicius, D.; Mukamel, S. Lindblad Equations for Strongly Coupled Populations and Coherences in Photosynthetic Complexes. *J. Chem. Phys.* **2009**, *130* (20), 204512. https://doi.org/10.1063/1.3142485.
- (51) Jang, S.; Cao, J.; Silbey, R. J. Fourth-Order Quantum Master Equation and Its Markovian Bath Limit. *J. Chem. Phys.* **2002**, *116* (7), 2705–2717. https://doi.org/10.1063/1.1445105.
- (52) Kim, Y. S.; Hochstrasser, R. M. Comparison of Linear and 2D IR Spectra in the Presence of Fast Exchange. *J. Phys. Chem. B* **2006**, *110* (17), 8531–8534. https://doi.org/10.1021/jp060935n.
- (53) Kim, Y. S.; Hochstrasser, R. M. The 2D IR Responses of Amide and Carbonyl Modes in Water Cannot Be Described by Gaussian Frequency Fluctuations. *J. Phys. Chem. B* **2007**, *111* (33), 9697–9701. https://doi.org/10.1021/jp074267x.
- (54) Abramavicius, D.; Mukamel, S. Exciton Dynamics in Chromophore Aggregates with Correlated Environment Fluctuations. *J. Chem. Phys.* **2011**, *134* (17), 174504. https://doi.org/10.1063/1.3579455.
- (55) Dahlbom, M.; Minami, T.; Chernyak, V.; Pullerits, T.; Sundström, V.; Mukamel, S. Exciton-Wave Packet Dynamics in Molecular Aggregates Studied with Pump-Probe Spectroscopy. *J. Phys. Chem. B* **2000**, *104* (16), 3976–3983. https://doi.org/10.1021/jp994172y.
- (56) Chuntonov, L.; Kuroda, D. G.; Ghosh, A.; Ma, J.; Hochstrasser, R. M. Quantum Beats and Coherence Decay in Degenerate States Split by Solvation. *J. Phys. Chem. Lett.* **2013**, *4* (11), 1866–1871. https://doi.org/10.1021/jz400826a.
- (57) Piryatinski, A.; Chernyak, V.; Mukamel, S. Vibrational-Exciton Relaxation Probed by Three-Pulse Echoes in Polypeptides. *Chem. Phys.* **2001**, *2*66 (2), 285–294. https://doi.org/10.1016/S0301-0104(01)00231-2.

PLEASE CITE THIS ARTICLE AS DOI: 10.1063/5.0216515

- Chuntonov, L.; Ma, J. Quantum Process Tomography Quantifies Coherence Transfer (58)Dynamics in Vibrational Exciton. J. Phys. Chem. B 2013, 117 (43), 13631–13638. https://doi.org/10.1021/jp4075493.
- (59)Edler, J.; Hamm, P. Two-Dimensional Vibrational Spectroscopy of the Amide I Band of Crystalline Acetanilide: Fermi Resonance, Conformational Substates, or Vibrational Self-Trapping? J. Chem. Phys. 2003, 119 (5), 2709–2715. https://doi.org/10.1063/1.1586694.
- (60)Chisler, E. V.; Davydov, V. Yu.; Goncharuk, I. N.; Ivanova, E. A. On Fermi Resonance Theory. Phys. Status Solidi B 1976, 78 (1), 359–370. https://doi.org/10.1002/pssb.2220780137.
- Seo, D. M.; Reininger, S.; Kutcher, M.; Redmond, K.; Euler, W. B.; Lucht, B. L. Role of Mixed (61)Solvation and Ion Pairing in the Solution Structure of Lithium Ion Battery Electrolytes. J. Phys. Chem. C 2015, 119 (25), 14038-14046. https://doi.org/10.1021/acs.jpcc.5b03694.
- Rubtsova, N. I.; Rubtsov, I. V. Vibrational Energy Transport in Molecules Studied by Relaxation-Assisted Two-Dimensional Infrared Spectroscopy. Annu. Rev. Phys. Chem. 2015, 66 (1), 717–738. https://doi.org/10.1146/annurev-physchem-040214-121337.
- (63)Thielges, M. C.; Fayer, M. D. Time-Dependent Fifth-Order Bands in Nominally Third-Order 2D IR Vibrational Echo Spectra. J. Phys. Chem. A 2011, 115 (34), 9714–9723. https://doi.org/10.1021/jp201516s.
- Strasfeld, D. B.; Shim, S.-H.; Zanni, M. T. Controlling Vibrational Excitation with Shaped Mid-(64)IR Pulses. Phys. Rev. Lett. 2007, 99 (3), 038102. https://doi.org/10.1103/PhysRevLett.99.038102.
- (65)Rector, K. D.; Kwok, A. S.; Ferrante, C.; Tokmakoff, A.; Rella, C. W.; Fayer, M. D. Vibrational Anharmonicity and Multilevel Vibrational Dephasing from Vibrational Echo Beats. J. Chem. Phys. **1997**, *106* (24), 10027–10036. https://doi.org/10.1063/1.474060.
- Roberts, S. T.; Loparo, J. J.; Tokmakoff, A. Characterization of Spectral Diffusion from Two-Dimensional Line Shapes. J. Chem. Phys. 2006, 125 (8), 084502. https://doi.org/10.1063/1.2232271.
- (67)Stenger, J.; Madsen, D.; Dreyer, J.; Nibbering, E. T. J.; Hamm, P.; Elsaesser, T. Coherent Response of Hydrogen Bonds in Liquids Probed by Ultrafast Vibrational Spectroscopy. J. Phys. Chem. A 2001, 105 (13), 2929–2932. https://doi.org/10.1021/jp003153h.
- Corcelli, S. A.; Lawrence, C. P.; Asbury, J. B.; Steinel, T.; Fayer, M. D.; Skinner, J. L. Spectral Diffusion in a Fluctuating Charge Model of Water. J. Chem. Phys. 2004, 121 (18), 8897–8900. https://doi.org/10.1063/1.1803532.
- Asbury, J. B.; Steinel, T.; Kwak, K.; Corcelli, S. A.; Lawrence, C. P.; Skinner, J. L.; Fayer, M. D. (69)Dynamics of Water Probed with Vibrational Echo Correlation Spectroscopy. J. Chem. Phys. 2004, 121 (24), 12431–12446. https://doi.org/10.1063/1.1818107.
- Cadioli, B.; Gallinella, E.; Coulombeau, C.; Jobic, H.; Berthier, G. Geometric Structure and Vibrational Spectrum of Tetrahydrofuran. J. Phys. Chem. 1993, 97 (30), 7844–7856. https://doi.org/10.1021/j100132a010.

### The Journal of Chemical Physics

This is the author's peer reviewed, accepted manuscript. However, the online version of record will be different from this version once it has been copyedited and typeset.

PLEASE CITE THIS ARTICLE AS DOI: 10.1063/5.0216515



(71) Kubo, R. A Stochastic Theory of Line Shape. In *Advances in Chemical Physics*; John Wiley & Sons, Ltd, 1969; pp 101–127. https://doi.org/10.1002/9780470143605.ch6.